Copper(I) complexes of 6,6′-disubstituted 2,2′-bipyridine dicarboxylic acids: new complexes for incorporation into copper-based dye sensitized solar cells (DSCs)†

Edwin C. Constable,* Ana Hernandez Redondo, Catherine E. Housecroft,* Markus Neuburger and Silvia Schaffner

Received 21st January 2009, Accepted 2nd June 2009
First published as an Advance Article on the web 7th July 2009
DOI: 10.1039/b901346f

Synthetic approaches to 6,6′-disubstituted-2,2′-bipyridine ligands bearing carboxylic acid substituents at the 4,4′ or 5,5′-positions are described. Copper(I) complexes with these ligands have been prepared for use in copper-based dye-sensitized solar cells. The single-crystal structures of 6,6′-dimethyl-2,2′-bipyridine-4,4′-dicarboxylic acid (H_2**4**), [H_3**6**][CF_3CO_2]·2CF_3CO_2H (H_2**6** = 6,6′-diphenyl-2,2′-bipyridine-4,4′-dicarboxylic acid) and 4[Cu(H_2**2**)(H**2**)]·3H_2O (H_2**2** = 6,6′-dimethyl-2,2′-bipyridine-5,5′-dicarboxylic acid) are described, as well as those of the intermediates (1*E*,5*E*)-1,6-di(2-furyl)hexa-1,5-diene-3,4-dione and 4,4′-di(2-furyl)-6,6′-dimethyl-2,2′-bipyridine (**3**), and the copper(I) complex [Cu(**3**)$_2$][PF_6]. The roles that classical and non-classical hydrogen bonding and π-stacking interactions play in determining the solid-state packing in these structures are discussed. Preliminary studies of DSCs with these complexes are reported.

Introduction

Carboxylate-functionalised complexes have become a popular choice for use in dye-sensitized solar cells (DSCs).[1–4] While ruthenium(II) complexes dominate the dyes studied to date, we have recently shown that efficient DSCs can be fabricated using carboxylate-derivatised copper(I) bis(2,2′-bipyridine) complexes.[5] This success has led us to a wider investigation of $[CuL_2]^+$ complexes where L is a bpy ligand functionalised in the 4,4′- or 5,5′-positions with carboxylic acid groups. A key structural requirement for the preparation of air-stable copper(I) complexes with 2,2′-bipyridine ligands is the presence of substituents at the 6- and 6′-positions[6] and in this paper we report compounds with either methyl or phenyl substituents at these positions. From a structural point of view, these ligands and complexes are of interest in their own right because of the propensity for hydrogen bond formation between adjacent $CO_2H\cdots HO_2C$ units. In addition, it is well established that co-crystallisation of carboxylic acids with heterocyclic bases may lead to supramolecular assemblies based upon O–H···N and C–H···O interactions.[7] In this paper, we describe the syntheses and copper(I) complexes of a series of 6,6′-dimethyl- or 6,6′-diphenyl-2,2′-bipyridines substituted in the 4,4′- or 5,5′-positions with carboxylic acid functionalities, as well as structural details for selected ligands and complexes.

Department of Chemistry, University of Basel, Spitalstrasse 51, CH 4056 Basel, Switzerland. E-mail: catherine.housecroft@unibas.ch; Fax: +41 61 267 1018; Tel: +41 61 267 1008

† CCDC reference numbers 717559–717565. For crystallographic data in CIF or other electronic format see DOI: 10.1039/b901346f

Experimental

General

^{1}H and ^{13}C NMR spectra were recorded at room temperature on Bruker Avance DRX 600 and 500 MHz spectrometers; chemical shifts are relative to residual solvent peaks with TMS δ 0 ppm. Infrared spectra were recorded on a Shimadzu FTIR-8400S spectrophotometer with solid samples on a Golden Gate diamond ATR accessory. Electron impact (EI), electrospray ionisation (ESI), and MALDI-TOF mass spectra were recorded using Finnigan MAT 95 and MAT LCQ and PerSeptive Biosystems Voyager mass spectrometers, respectively. Electronic absorption spectra were recorded on a Varian-Cary 5000 spectrophotometer. Electrochemical measurements were performed with an Eco Chemie Autolab PGSTAT 20 system using glassy carbon working and platinum auxiliary electrodes with a silver wire as pseudo-reference electrode; solvents (see Experimental section) were purified. With the exception of Na_3[Cu(**6**)$_2$], 0.1 M [^{n}Bu$_4$N][PF_6] was used as supporting electrolyte, and ferrocene (Fc) was added at the end of each experiment as an internal reference. For Na_3[Cu(**6**)$_2$], the supporting electrolyte was 0.1M $NaClO_4$ and measurements were made relative to Ag/AgCl, then corrected to be with respect to Fc/Fc^+.

Diethyl 6,6′-dimethyl-2,2′-bipyridine-5,5′-dicarboxylate (1)

The method is based on that reported for the synthesis of diethyl 4,4′,6,6′-tetramethyl-2,2′-bipyridine-5,5′-dicarboxylate.[8] Ethyl 2-methylnicotinate (9.34 cm^3, 60.5 mmol) and Pd/C (5%, 1.35 g) were heated at reflux for 10 d under an inert atmosphere. After cooling the reaction mixture to room temperature, acetone (20 cm^3) was added and the Pd/C was removed by filtration. The filtrate was evaporated to dryness. After standing overnight in the refrigerator, the brown–black solid was recrystallised

from MeOH, and **1** was isolated as pale brown needles (0.31 g, 0.93 mmol, 1.5%). ^{1}H NMR (500 MHz, $CDCl_3$) δ/ppm 8.41 (d, J = 8.1 Hz, 2H, H^{A3}), 8.33 (d, J = 8.1 Hz, 2H, H^{A4}), 4.41 (q, J = 7.1 Hz, 4H, H^{CH2CH3}), 2.92 (s, 6H, H^{Me}), 1.43 (t, J = 7.1 Hz, 6H, H^{CH2CH3}). ^{13}C NMR (125 MHz, $CDCl_3$) δ/ppm 166.5 ($C^{C=O}$), 159.5 (C^{A6}), 156.6 (C^{A2}), 139.5 (C^{A4}), 125.7 (C^{A5}), 118.8 (C^{A3}), 61.3 (C^{CH2CH3}), 25.1 (C^{Me}), 14.3 (C^{CH2CH3}). MALDI-MS m/z 330.1 [M + 2H]$^+$ (calc. 328.1). IR: ν/cm^{-1} 2976w, 2933w, 1716s, 1584s, 1547m, 1445m, 1428m, 1390m, 1353m, 1273s, 1249s, 1139m, 1114m, 1078s, 1020m, 986m, 8506s, 773s, 723m. Found: C, 65.89; H, 6.20; N, 8.54; $C_{18}H_{20}N_2O_4$ requires C, 65.84; H, 6.14; N, 8.53%.

6,6′-Dimethyl-2,2′-bipyridine-5,5′-dicarboxylic acid (H_2**2**)

Compound **1** (0.27 g, 0.82 mmol) was partially dissolved in a H_2O–EtOH (20 cm^3, 1 : 1 vol.) solution which contained KOH (0.46 g, 8.2 mmol). The mixture was heated at reflux for 12 h. After cooling to room temperature, the solution was partially evaporated under reduced pressure and the pH was adjusted to 2 with 1 M aqueous HCl to give a white precipitate. After filtration, H_2**2** was collected as a white solid (0.221 g, 0.813 mmol, 99%). ^{1}H NMR (500 MHz, DMSO-d_6) δ/ppm 8.35 (m, 4H, H^{A3+A4}), 2.82 (s, 6H, H^{Me}). ^{13}C NMR (126 MHz, DMSO-d_6) δ/ppm 167.6 ($C^{C=O}$), 158.6 (C^{A6}), 155.5 (C^{A2}), 139.7 (C^{A4}), 126.4 (C^{A5}), 118.5 (C^{A3}), 24.7 (C^{Me}). EI-MS m/z 272.1 [M]$^+$ (calc. 272.1). IR (ν/cm^{-1}) 3000w, 2893w, 2796w, 2645w, 2527w, 1688s, 1583s, 1544s, 1435m, 1404s, 1379m, 1349 (w), 1285s, 1258s, 1219m, 1140m, 1119m, 1079m, 1033w, 986w, 926m, 851s, 774s, 666s, 641m, 621w. UV-VIS (MeOH) λ_{max}/nm (ε/dm^3 mol^{-1} cm^{-1}) 212 (13000), 250 (13500), 305 (26000). Found: C, 59.50; H, 4.58; N, 9.82; $C_{14}H_{12}N_2O_4 \cdot 0.5H_2O$ requires C, 59.78; H, 4.66; N, 9.96%.

(1*E*,5*E*)-1,6-Di(2-furyl)hexa-1,5-diene-3,4-dione

The synthesis followed a literature method,[9] although spectroscopic data have not previously been reported. (1*E*,5*E*)-1,6-di(2-furyl)hexa-1,5-diene-3,4-dione was isolated as an orange crystalline solid in 11.7% yield. ^{1}H NMR (500 MHz, $CDCl_3$, ring B = furan) δ/ppm 7.61 (d, J = 15.9 Hz, 2H, H^1), 7.57 (dd, J = 1.7, 0.4 Hz, 2H, H^{B5}), 7.31 (d, J = 15.9 Hz, 2H, H^2), 6.80 (d, J = 3.5 Hz, 2H, H^{B3}), 6.53 (dd, J = 3.5, 1.8 Hz, 2H, H^{B4}). ^{13}C NMR (126 MHz, $CDCl_3$) δ/ppm 188.7 ($C^{C=O}$), 151.6 (C^{B2}), 146.2 (C^{B5}), 133.1 (C^1), 117.9 (C^{B3}), 117.4 (C^2), 113.1 (C^{B4}). EI-MS m/z 242.1 [M]$^+$ (calc. 242.1). IR (ν/cm^{-1}) 3123w, 1662m, 1585m, 1543m, 1471m, 1388w, 1289m, 1265m, 1200m, 1068w, 995m, 974s, 926s, 881m, 850m, 831m, 811m, 746s, 637s, 588s, 548s. Found: C, 69.23; H, 4.20; $C_{14}H_{10}O_4$ requires C, 69.42; H, 4.16%.

4,4′-Di(2-furyl)-6,6′-dimethyl-2,2′-bipyridine (3)

The preparation of **3** was based on the reported method,[10,11] although few characterisation data for **3** were available. (1*E*,5*E*)-1,6-Di(2-furyl)hexa-1,5-diene-3,4-dione (0.500 g, 2.07 mmol), 1-acetonylpyridinium chloride (0.708 g, 4.132 mmol) and ammonium acetate (1.0 g, 13 mmol) were heated at reflux in MeOH (20 cm^3) for 12 h. The solution was allowed to cool to room temperature, and the off-white precipitate was collected by filtration and washed with cold MeOH. **3** was isolated as a white solid (0.361 g, 1.14 mmol, 55%). ^{1}H NMR (500 MHz, $CDCl_3$) δ/ppm 8.61 (s, 2H, H^{A3}), 7.58 (dd, J = 1.7, 0.6 Hz, 2H, H^{B5}), 7.49 (d, J = 1.1 Hz, 2H, H^{A5}), 7.12 (d, J = 1.4 Hz, 2H, H^{B3}), 6.56 (dd, J = 3.5, 1.7 Hz, 2H, H^{B4}), 2.75 (s, 6H, H^{Me}). ^{13}C NMR (126 MHz, $CDCl_3$) δ/ppm 158.3 (C^{A6}), 151.5 (C^{B2}), 143.9 (C^{B5}), 139.4 (C^{A4}), 117.6 (C^{A5}), 113.7 (C^{A3}), 112.3 (C^{B4}), 109.9 (C^{B3}), 24.3 (C^{Me}) (C^{A2} not observed). EI-MS m/z 316.1 [M]$^+$ (calc. 316.1). IR (ν/cm^{-1}) 3115w, 2370w, 1603m, 1574m, 1548s, 1485m, 1410m, 1374m, 1359m, 1218m, 1161m, 1016s, 985m, 930m, 865m, 848m, 813s, 744s, 700s, 669m, 595s. Satisfactory analysis could not be obtained.

6,6′-Dimethyl-2,2′-bipyridine-4,4′-dicarboxylic acid (H_2**4**)

Compound H_2**4** was prepared from **3** as previously described, and the ^{1}H NMR and UV-VIS spectra agreed with literature data.[11] ^{13}C NMR (126 MHz, DMSO-d_6) δ/ppm 166.3 ($C^{C=O}$), 159.3 (C^{A6}), 155.1 (C^{A2}), 139.4 (C^{A4}), 122.8 (C^{A5}), 116.8 (C^{A3}), 24.2 (C^{Me}). EI-MS m/z 272.1 [M]$^+$ (calc. 272.1), 228.1 [M – COO]$^+$ (calc. 228.1). IR (ν/cm^{-1}) 3093w, 2916w, 2854w, 2615w, 2545w, 1836w, 1697s, 1566s, 1427s, 1396m, 1296s, 1218m, 1095w, 910m, 763m. Found: C, 61.17; H 4.90; N, 10.38; $C_{14}H_{12}N_2O_4$ requires C, 61.76; H, 4.44; N, 10.29%.

4,4′-Di(2-furyl)-6,6′-diphenyl-2,2′-bipyridine (5)

1,6-Di(2-furyl)hexa-1,5-diene-3,4-dione (0.500 g, 2.07 mmol), *N*-phenacylpyridinium bromide (1.149 g, 4.132 mmol) and ammonium acetate (1.0 g, 13 mmol) were heated at reflux in EtOH (20 cm^3) for 12 h. The solution was allowed to cool to room temperature, and the off-white precipitate was collected by filtration and washed with cold EtOH. **5** was collected as a white solid (0.464 g, 1.05 mmol, 51%). ^{1}H NMR (500 MHz, $CDCl_3$) δ/ppm 8.82 (d, J = 1.4 Hz, 2H, H^{A3}), 8.23 (d, J = 7.4 Hz, 4H, H^{C2}), 8.07 (d, J = 1.4 Hz, 2H, H^{A5}), 7.63 (d, J = 1.6 Hz, 2H, H^{B5}), 7.57 (m, 4H, H^{C3}), 7.49 (m, 2H, H^{C4}), 7.11 (d, J = 3.4 Hz, 2H, H^{B3}), 6.60 (dd, J = 3.4, 1.7 Hz, 2H, H^{B4}). ^{13}C NMR (126 MHz, $CDCl_3$) δ/ppm 157.1 (C^{A6}), 156.1 (C^{A2}), 151.9 (C^{B2}), 143.8 (C^{B5}), 139.4 (C^{C1}), 139.2 (C^{A4}), 129.2 (C^{C4}), 128.8 (C^{C3}), 127.1 (C^{C2}), 114.8 (C^{A5}), 114.2 (C^{A3}), 112.2 (C^{B4}), 109.1 (C^{B3}). EI-MS m/z 440.2 [M]$^+$ (calc. 440.2). IR (ν/cm^{-1}) 3040w, 1601m, 1570w, 1543m, 1489w, 1404w, 1366w, 1215w, 1153w, 1007m, 918w, 868m, 814w, 772m, 729m, 687s, 590s, 513s, 486s, 455s, 409s. Found: C 78.87, H 4.42, N 6.02; $C_{30}H_{20}N_2O_2 \cdot H_2O$ requires C 78.59, H 4.84, N 6.11%.

6,6′-Diphenyl-2,2′-bipyridine-4,4′-dicarboxylic acid (H_2**6**)

$KMnO_4$ (4.95 g, 31.3 mmol) was added to a warmed mixture of **5** (1.06 g, 2.42 mmol), ^{t}BuOH (145 cm^3) and H_2O (30 cm^3). After heating at reflux overnight, the mixture was filtered through Celite. The filtrate was evaporated to *ca.* 50 cm^3, the pH adjusted to 2 with 2 M HCl, and the white precipitate that formed was separated by filtration. H_2**6** was isolated as a white solid (0.62 g, 1.55 mmol, 64%). ^{1}H NMR (600 MHz, CF_3CO_2D) δ/ppm 9.22 (s, 2H, H^{A3}), 9.00 (s, 2H, H^{A5}), 8.19 (d, J = 7.2 Hz, 4H, H^{C2}), 7.82 (t, 2H, J = 7.3 Hz, H^{C4}), 7.77 (t, J = 7.4 Hz, 4H, H^{C3}). ^{13}C NMR (151 MHz, CF_3CO_2D) δ/ppm 169.2 ($C^{C=O}$), 160.3 (C^{A6}), 148.2 (C^{A2}), 146.4 (C^{A4}), 135.6 (C^{C4}), 134.0 (C^{C1}), 132.3 (C^{C3}), 129.4 (C^{C2}), 128 1 (C^{A5}), 123.5 (C^{A3}). ESI-MS m/z 397.2 [M + H]$^+$ (calc. 397.1). IR (ν/cm^{-1}) 2978w, 2831w, 2561w, 2361 w), 1690s, 1551s, 1427m, 1389s, 1296m, 1250s, 1142m, 895m, 756s, 679s. Satisfactory elemental analysis could not be obtained.

[Cu(H$_2$2)$_2$]Cl

The procedure was adapted from the literature.[8] An aqueous solution (2 cm^3) of H$_2$**2** (0.090 g, 0.33 mmol) was warmed to 70 °C, and 15 drops of 1 M aqueous NaOH were added to the solution. An aqueous solution (2 cm^3) of CuSO$_4$·5H$_2$O (0.042 g, 0.17 mmol) was then added, followed by a further addition of 20 drops of 1 M aqueous NaOH. An aqueous solution (0.3 cm^3) of ascorbic acid (0.044 g, 0.25 mmol) was added to the reaction mixture and the solution immediately turned dark red. The pH of the solution was adjusted to 2 by adding 1 M aqueous HCl to precipitate the product. After filtration, [Cu(H$_2$**2**)$_2$]Cl was isolated as a red solid (0.070 g, 0.11 mmol, 33%). ^{1}H NMR (500 MHz, CD$_3$OD) δ/ppm 8.54 (s, 8H, H^{A3+A4}), 2.57 (s, 12H, H^{Me}). ESI-MS m/z 605.1 [M − Cl]$^+$ (calc. 607.1). IR (ν/cm^{-1}) 3526w, 2916w, 1712m, 1582m, 1404w, 1381w, 1265m, 1157s, 1095w, 980w, 957w, 926w, 849m, 772s, 664w, 579m, 502m, 463s, 447s. UV-VIS (MeOH) λ_{max}/nm (ε/dm^3 mol^{-1} cm^{-1}) 214 (74400), 274 (47000), 314 (60000), 482 (8000). $E°$(MeOH)/V *vs.* Fc: +0.53 (quasi-reversible). Found: C 52.94, H 4.25, N 8.62; C$_{28}$H$_{24}$ClCuN$_4$O$_8$ requires C 52.26, H 3.76, N 8.71%.

[Cu(3)$_2$][PF$_6$]

A solution of [Cu(CH$_3$CN)$_4$][PF$_6$] (19 mg, 0.050 mmol) in CH$_3$CN (2 cm^3) was added to a solution of **3** (31.6 mg, 0.100 mmol) in CHCl$_3$ (5 cm^3) resulting in a change from colourless to red. Upon addition of Et$_2$O to the solution, a red precipitate formed. After filtration, [Cu(**3**)$_2$][PF$_6$] was isolated as a red solid (39 mg, 0.046 mmol, 46%). ^{1}H NMR (500 MHz, CDCl$_3$) δ/ppm 8.42 (s, 4H, H^{A3}), 7.68 (m, 8H, H^{A5+B5}), 7.24 (d, J = 3.6 Hz, 4H, H^{B3}), 6.66 (dd, J = 2.9, 1.5 Hz, 4H, H^{B4}), 2.29 (s, 12H, H^{Me}). ESI-MS m/z 695.8 [M − PF$_6$]$^+$ (calc. 695.2). IR (ν/cm^{-1}) 3115w, 2949w, 2912w, 2361w, 2334w, 1610m, 1547m, 1489m, 1441w, 1371w, 1250w, 1221w, 1159w, 1078w, 1020m, 937w, 932w, 885w, 872w, 835s, 739s, 704m, 673w. UV-VIS (CH$_3$CN) λ_{max}/nm (ε/dm^3 mol^{-1} cm^{-1}) 274 (67000), 289 (71000), 493 (4100). $E°$(MeCN)/V *vs.* Fc: +0.29 (reversible). Found: C, 55.83; H, 3.77; N, 6.36; C$_{40}$H$_{32}$CuF$_6$N$_4$O$_4$P·H$_2$O requires C, 55.91; H, 3.99; N, 6.52%.

[Cu(H$_2$4)$_2$]Cl

The procedure was as for [Cu(H$_2$**2**)$_2$]Cl, using H$_2$**4** (89.7 mg, 0.33 mmol) and CuSO$_4$·5H$_2$O (0.042 g, 0.17 mmol). [Cu(H$_2$**4**)$_2$]Cl was isolated as a red solid (58 mg, 0.090 mmol, 27%). ^{1}H NMR (500 MHz, CD$_3$OD) δ/ppm 8.91 (s, 4H, H^{A3}), 8.12 (s, 4H, H^{A5}), 2.32 (s, 12H, H^{Me}). ESI-MS m/z 607.2 [M − Cl]$^+$ (calc. 607.1). IR (ν/cm^{-1}) 3180w, 1712s, 1558s, 1434m, 1388m, 1265m, 1218m, 894m, 763s, 671 m. UV-VIS (MeOH) λ_{max}/nm (ε/dm^3 mol^{-1} cm^{-1}) 202 (34300), 252 (27200), 268 (25000), 319 (35400), 483 (9900). $E°$(MeOH)/V *vs.* Fc +0.42 (quasi-reversible). Found: C, 47.46; H, 3.99; N, 7.90; C$_{28}$H$_{24}$ClCuN$_4$O$_8$·4H$_2$O requires C, 47.00; H, 4.51; N, 7.83%.

[Cu(5)$_2$][PF$_6$]

The method was as for [Cu(**3**)$_2$][PF$_6$], starting with [Cu(CH$_3$CN)$_4$][PF$_6$] (84.6 mg, 0.227 mmol) in CH$_3$CN (3 cm^3) and **5** (200 mg, 0.455 mmol) in CHCl$_3$ (7 cm^3). [Cu(**5**)$_2$][PF$_6$] was isolated as a dark green solid (336 mg, 0.309 mmol, 68%). ^{1}H NMR (600 MHz, CD$_2$Cl$_2$ with added K$_2$CO$_3$) δ/ppm 8.13 (s, 4H, H^{A3}), 7.77 (d, J = 1.1 Hz, 4H, H^{B5}), 7.75 (s, 4H, H^{A5}), 7.58 (d, J = 7.4 Hz, 8H, H^{C2}), 7.21 (d, J = 3.4 Hz, 4H, H^{B3}), 7.06 (t, J = 7.4 Hz, 4H, H^{C4}), 6.91 (t, J = 7.6 Hz, 8H, H^{C3}), 6.73 (dd, J 3.3, 1.7 Hz, 4H, H^{B4}). ^{13}C NMR (151 MHz, CD$_2$Cl$_2$) δ/ppm 157.8 (C^{A6}), 153.9 (C^{A2}), 150.9 (C^{B2}), 145.7 (C^{B5}), 139.7 (C^{A4}), 138.8 (C^{C1}), 129.9 (C^{C4}), 128.1 (C^{C2+C3}), 119.2 (C^{A5}), 115.5 (C^{A3}), 113.5 (C^{B4}), 111.5 (C^{B3}). ESI-MS m/z 943.0 [M − PF$_6$]$^+$ (calc. 943.2). IR (ν/cm^{-1}) 3122w, 3059w, 1735w, 1608s, 1540m, 1486m, 1454w, 1440w, 1429w, 1407w, 1371w, 1308w, 1244w, 1222m, 1157w, 1076w, 1016m, 937w, 920w, 884m, 833s, 769s, 738s, 692s, 642m, 590m, 554s. UV-VIS (CHCl$_3$) λ_{max}/nm (ε/dm^3 mol^{-1} cm^{-1}) 244 (35000), 282 (36000), 313 (48000), 432 (4000), 587 (2400). $E°$(MeCN)/V *vs.* Fc: +0.27 (reversible). Found: C, 63.63; H, 3.72; N, 4.79; C$_{60}$H$_{40}$CuF$_6$N$_4$O$_4$P·2.4H$_2$O requires C, 63.62; H, 3.99; N, 4.95%.

[Cu(H$_2$6)$_2$]Cl

The procedure was as for [Cu(H$_2$**2**)$_2$]Cl, using H$_2$**6** (39.6 mg, 0.100 mmol) and CuSO$_4$·5H$_2$O (12.5 mg, 0.0500 mmol). [Cu(H$_2$**6**)$_2$]Cl was isolated as a green solid (31.1 mg, 0.035 mmol, 35%). ^{1}H NMR (see text) (600 MHz, D$_2$O) δ/ppm 8.08 (s, 4H, H^{A3}), 6.99 (m, 12H, H^{A5+C2}), 6.49 (m, 4H, H^{C4}), 6.40 (m, 8H, H^{C3}). MS see text. IR (ν/cm^{-1}) 3059w, 2357w, 1716s, 1608w, 1553s, 1456m, 1437m, 1377m, 1296w, 1217s, 1026w, 999w, 901m, 841m, 764s, 737m, 692s, 640m. UV-VIS (see text, H$_2$O): λ_{max}/nm (ε/dm^3 mol^{-1} cm^{-1}) 296 (10000), 343 (11000), 437 (2000), 608 (1170). $E°$(see text, H$_2$O)/V *vs.* Fc: 0.00 (reversible). Found: C, 62.82; H, 3.86; N, 6.05; C$_{48}$H$_{31}$ClCuN$_4$O$_8$·1.7H$_2$O requires C, 62.57; H, 3.76; N, 6.08%.

Crystal structure determinations

Data were collected on a Bruker-Nonius Kappa CCD instrument; data reduction, solution and refinement used the programs COLLECT,[12] DENZO/SCALEPACK,[13] SIR92,[14] and CRYSTALS.[15] The positions of the H atoms bonded to O or N atoms were located in the difference maps. Structures have been analysed using Mercury v. 1.4.2.[16] ORTEP figures were drawn using Ortep-3 for Windows.[17]

(1*E*,5*E*)-1,6-Di(2-furyl)hexa-1,5-diene-3,4-dione

C$_{14}$H$_{10}$O$_4$, M = 242.23, colourless plate, monoclinic, space group $C2/c$, a = 37.426(1), b = 3.7745(2), c = 18.0118(7) Å, β = 118.174(2)°, U = 2242.96(18) Å^3, Z = 8, D_c = 1.435 Mg m^{-3}, μ(Mo-Kα) = 0.106 mm^{-1}, T = 173 K, 2556 reflections collected. Refinement of 1651 reflections (164 parameters) with $I > 1.9\sigma(I)$ converged at final $R1$ = 0.0470 ($R1$ all data = 0.0717), $wR2$ = 0.0519 ($wR2$ all data = 0.0648), R_{int} = 0.026, gof = 1.138.

4,4′-Di(2-furyl)-6,6′-dimethyl-2,2′-bipyridine (3)

C$_{20}$H$_{16}$N$_2$O$_2$, M = 316.36, colourless plate, orthorhombic, space group $Pcab$, a = 6.5194(1), b = 12.1847(2), c = 19.5707(3) Å, U = 1554.64(4) Å^3, Z = 4, D_c = 1.352 Mg m^{-3}, μ(Mo-Kα) = 0.089 mm^{-1}, T = 173 K, 1855 reflections collected. Refinement of 1101 reflections (109 parameters) with $I > 2.5\sigma(I)$ converged at final $R1$ = 0.0408 ($R1$ all data = 0.0641), $wR2$ = 0.0349 ($wR2$ all data = 0.0416), R_{int} = 0.071, gof = 1.121.

6,6′-Dimethyl-2,2′-bipyridine-4,4′-dicarboxylic acid ($H_2$4)

$C_{14}H_{12}N_2O_4$, M = 272.26, colourless plate, triclinic, space group $P\bar{1}$, a = 3.8591(6), b = 8.111(1), c = 10.607(2) Å, α = 73.344(9), β = 84.983(7), γ = 77.881(10)°, U = 310.83(8) Å^3, Z = 1, D_c = 1.454 Mg m^{-3}, μ(Mo-Kα) = 0.109 mm^{-1}, T = 173 K, 1468 reflections collected. Refinement of 1461 reflections (91 parameters) with $I > 2.0\sigma(I)$ converged at final $R1$ = 0.0513 ($R1$ all data = 0.0834), $wR2$ = 0.0870 ($wR2$ all data = 0.1174), R_{int} = 0.030, gof = 1.040.

4,4′-Di(2-furyl)-6,6′-diphenyl-2,2′-bipyridine (5)

$C_{30}H_{20}N_2O_2$, M = 440.50, colourless plate, trigonal, space group $R\bar{3}$, $a = b$ = 33.495(2), c = 5.1499(3) Å, U = 5003.7(5) Å^3, Z = 9, D_c = 1.316 Mg m^{-3}, μ(Mo-Kα) = 0.083 mm^{-1}, T = 173 K, 2084 reflections collected. Refinement of 2064 reflections (155 parameters) with $I > 2.0\sigma(I)$ converged at final $R1$ = 0.0375 ($R1$ all data = 0.0773), $wR2$ = 0.0554 ($wR2$ all data = 0.0800), R_{int} = 0.050, gof = 1.018.

4[Cu($H_2$2)(H2)]·3H_2O

$C_{112}H_{98}Cu_4N_{16}O_{35}$, M = 2482.28, purple plate, monoclinic, space group $C2/c$, a = 19.3405(4), b = 19.6142(4), c = 15.5801(3) Å, β = 114.0211(9)°, U = 5398.4(2) Å^3, Z = 2, D_c = 1.527 Mg m^{-3}, μ(Mo-Kα) = 0.871 mm^{-1}, T = 173 K, 6190 reflections collected. Refinement of 4532 reflections (449 parameters) with $I > 2.0\sigma(I)$ converged at final $R1$ = 0.0360 ($R1$ all data = 0.0468), $wR2$ = 0.0364 ($wR2$ all data = 0.0394), R_{int} = 0.033, gof = 1.044.

[$H_3$6][CF_3CO_2]·2CF_3CO_2H

$C_{30}H_{19}F_9N_2O_{10}$, M = 738.47, colourless needle, triclinic, space group $P\bar{1}$, a = 9.0489(7), b = 9.8221(8), c = 17.542(1) Å, α = 93.451(5), β = 98.501(5), γ = 95.971(5)°, U = 1529.1(2) Å^3, Z = 2, D_c = 1.604 Mg m^{-3}, μ(Mo-Kα) = 0.155 mm^{-1}, T = 173 K, 9445 reflections collected. Refinement of 4614 reflections (505 parameters) with $I > 1.0\sigma(I)$ converged at final $R1$ = 0.0833 ($R1$ all data = 0.1798), $wR2$ = 0.0638 ($wR2$ all data = 0.0966), R_{int} = 0.075, gof = 1.285.

[Cu(3)$_2$][PF_6]

$C_{40}H_{32}CuF_6N_4O_4P$, M = 841.23, orange plate, triclinic, space group $P\bar{1}$, a = 8.9016(2), b = 10.9570(3), c = 19.0865(4) Å, α = 81.724(1), β = 81.0409(1), γ = 88.743(1)°, U = 1819.78(8) Å^3, Z = 2, D_c = 1.535 Mg m^{-3}, μ(Mo-Kα) = 0.724 mm^{-1}, T = 173 K, 13054 reflections collected. Refinement of 7298 reflections (505 parameters) with $I > 3.0\sigma(I)$ converged at final $R1$ = 0.0378 ($R1$ all data = 0.0715), $wR2$ = 0.0408 ($wR2$ all data = 0.0594), R_{int} = 0.051, gof = 1.106.

Preparation and evaluation of solar cells

Nanocrystalline titanium dioxide electrodes were prepared by doctor blading a colloidal TiO_2 paste (Solaronix Nanooxide-T, colloidal anatase) on the conductive transparent surface of a piece of glass (F-doped SnO_2, FTO, Hartford glass company, Tec 8, 8Ω cm^{-2}) that had been cut to 0.9 × 2.0 cm and cleaned with water and ethanol. The FTO-coated glass was covered with two layers of parallel adhesive tape 0.5 cm apart to control the thickness and the area of the TiO_2 film (0.9 × 0.5 cm). The colloidal paste was applied between the tapes by rolling a glass rod on the surface. The film thickness was measured with a profilometer (Dektak) and was 6.0 ± 0.5 μm. After annealing at 450 °C for 30 min, the slides were dipped into a solution of the dye in an appropriate solvent (see Table 1) for several hours. The cells were constructed using 0.5 M LiI, 0.05 M I_2, 0.5 M 1-methylbenzimidazole and 0.6 M 1-butyl-3-methylimidazolinium iodide in 3-methoxypropionitrile as electrolyte. The electrolyte was chosen to give the best possible comparison to the state-of-the-art optimized systems based on N719. Cathode electrodes were constructed from FTO glass pieces of the same dimensions as the anodes platinized by treatment with 5 mM $H_2[PtCl_6]$ in propan-2-ol followed by heating to 380 °C for 15 min. The anode and cathode were assembled using Surlyn (Dupont) plastic and the seal made by heating to 110–120 °C while pressing the two together. Measurements were made with irradiation from the rear using a lamp with intensity 100 mW cm^{-2} (1 sun). The standard dye N719 was purchased from Solaronix.

Table 1 Current–voltage characteristic data for DSCs constructed with copper(I) complexes as photosensitizers. Cells were constructed as described in the experimental section

Compound (solvent)	J_{sc}/mA cm^{-2}	V_{oc}/mV	FF	η_{global} (%)	λ_{max}/nm (soln)	λ_{max}/nm (dye)
[Cu($H_2$2)$_2$]Cl (MeOH)	1.21	570	0.65	0.45	482	480
[Cu($H_2$4)$_2$]Cl (MeOH)	1.15	530	0.68	0.41	483	492
[Cu($H_2$6)$_2$]Cl[a] (DMSO)	0.69	484	0.63	0.21	437, 608	494, 604
[Cu(3)$_2$][PF_6] ($CHCl_3$)	0.46	490	0.62	0.14	493	494
N719 (MeCN)	11.3	750	0.67	5.0	534	392, 530

[a] Solution UV-VIS data are for the sodium salt, see text.

Results and discussion

Ligand synthesis and characterisation

Entry into the 6,6′-dimethyl-5,5-dicarboxylic acid series is achieved through the convenient (but low-yielding) oxidative dimerisation of ethyl 2-methylnicotinate with palladium/charcoal.[8,18,19] Ligand H_2**2** was prepared in near quantitative yield by the saponification of **1**[8] under basic conditions, and was fully characterised by routine spectroscopic and mass spectrometric methods. For H_2**4** and H_2**6**, the strategy outlined in Scheme 2 was employed; this has previously been applied to the synthesis of H_2**4**. For H_2**4**, our ^{1}H NMR and UV-VIS spectroscopic data agreed with those published,[11] and the ^{13}C NMR spectrum exhibited the number of resonances expected and was fully assigned by 2D NMR techniques.

X-Ray quality crystals of the dione precursor shown in Scheme 2 readily formed from an ethanol solution of the compound, and a search of the CSD[16] revealed that its structure had not previously been reported. The molecular structure of the dione is shown in Fig. 1. The asymmetric unit contains two independent, centrosymmetric molecules, and all bond distances and angles are unexceptional. Each molecule is planar (deviations of atoms

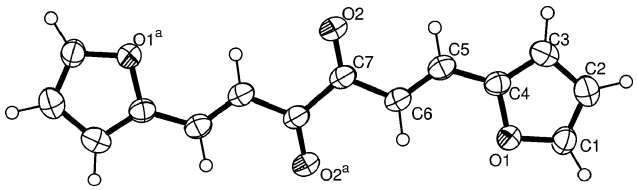

Fig. 1 Structure of one of the independent molecules of (1*E*,5*E*)-1,6-di(2-furyl)hexa-1,5-diene-3,4-dione; ellipsoids are plotted at the 50% level. Selected bond distances (Å): C5–C6 1.336(3), C4–C5 1.429(3), C6–C7 1.467(3), C7–C7^{a} 1.532(4), C7–O2 1.220(2), C1–O1 1.373(2), C4–O1 1.376(2); symmetry code a = 1 − *x*, 1 − *y*, −*z*. Bond lengths in the second independent molecule are similar.

from the least squares plane through each molecule < 0.2 Å), and the planes through the two independent molecules are almost parallel (angle subtended = 3.4°). The molecules are stacked in an offset manner, and continuation of this stacking arrangement generates columns. Molecules in adjacent stacks interact with each other through weak O···H–C contacts (C1H11···O4^{i} = 2.68, O2···H91^{i}C9^{i} = 2.61, C2H21···O4^{ii} = 2.63 Å) and C–H···π_{alkene} interactions (C3H31···C13^{iii} = 2.89, C3H31···C12^{iii} =3.24 Å) (symmetry codes i = *x*, 1 + *y*, *z*; ii = $\frac{1}{2}$ − *x*, $\frac{1}{2}$ + *y*, $-\frac{1}{2}$ − *z*; iii = *x*, −*y*, $-\frac{1}{2}$ + *z*). Such weak interactions are well established as important components in solid-state supramolecular assemblies.[20–25] The overall supramolecular assembly is a herring-bone like array (Fig. 2), with an angle of 58.4° between the planes through molecules in adjacent stacks.

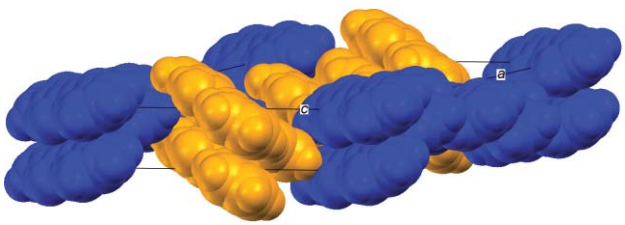

Fig. 2 Packing of dione molecules (see text).

Ligands H_2**4** and H_2**6** were prepared by permanganate oxidation of 4,4′-di(2-furyl)-6,6′-dimethyl-2,2′-bipyridine (**3**) and 4,4′-di(2-furyl)-6,6′-diphenyl-2,2′-bipyridine (**5**), respectively.[26] The intermediate compounds were fully characterised. Each exhibited a parent ion in the EI mass spectrum (*m*/*z* 316.1 for **3**, and *m*/*z* 440.2 for **5**). The ^{1}H NMR spectra of **3** and **5** are readily distinguished by the presence of a signal at δ 2.75 ppm for the methyl groups in **3**, and diagnostic signals for the phenyl substituents (ring C, Scheme 1) in the spectrum of **5**. The chemical shifts of the resonances assigned to the bipyridine rings (A, Scheme 1) and furan rings (B) are similar in **3** and **5**, with the exception of the signal for proton H^{A5} which appears at δ 7.49 ppm in **3** and at δ 8.07 ppm in **5**. This observation is consistent with the deshielding effect of the 6-phenyl substituent on H^{A5}. The ^{13}C NMR spectra were assigned using 2D techniques. Both compounds yielded X-ray quality crystals, grown by slow evaporation of chloroform solutions of the ligands. The centrosymmetric structures are shown in Fig. 3(a) and 4(a), respectively. The bpy unit in each compound adopts the expected *trans*-configuration. Both **3** and **5** are close to being planar. In **3**, the angle between the least squares planes of the pyridine and

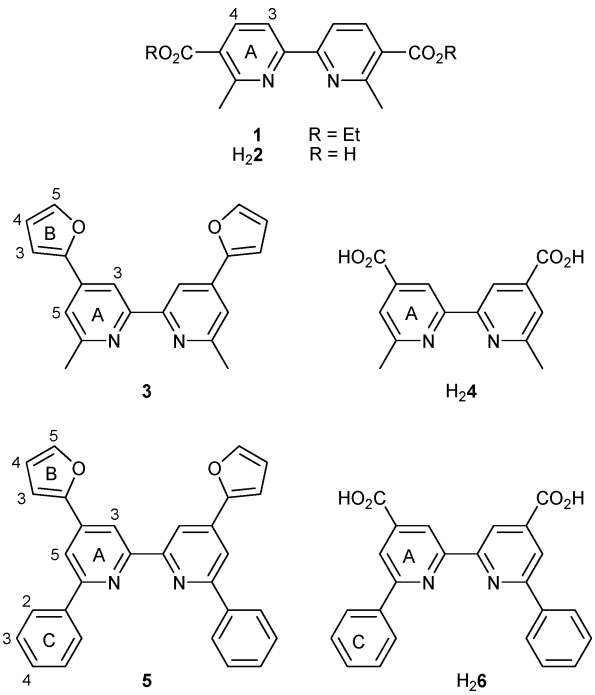

Scheme 1 Ligand structures and ring labelling for NMR spectroscopy.

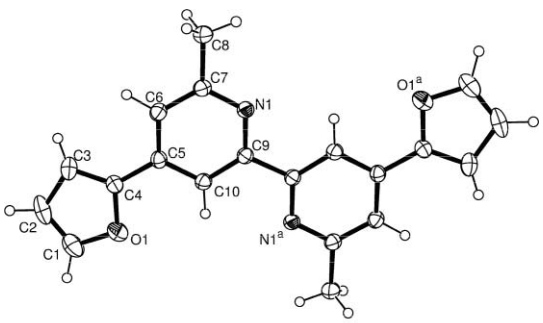

(a)

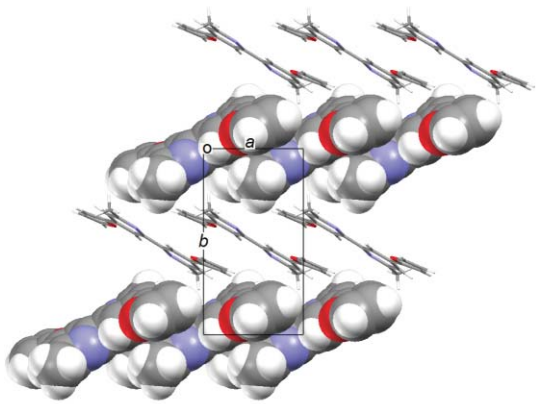

(b)

Fig. 3 (a) Molecular structure of compound **3** with ellipsoids plotted at the 40% level. Selected bond parameters (Å and °): C7–C8 1.503(2), C9–C9^{i} 1.493(3), C4–C5 1.455(2), O1–C1 1.358(2), O1–C4 1.370(2), C1–C2 1.326(3), C2–C3 1.449(3), C3–C4 1.349(3); C1–O1–C4 106.8(2) (symmetry code: i = 2 − *x*, −*y*, 1 − *z*). (b) Packing of molecules of **3** is dominated by π-stacking.

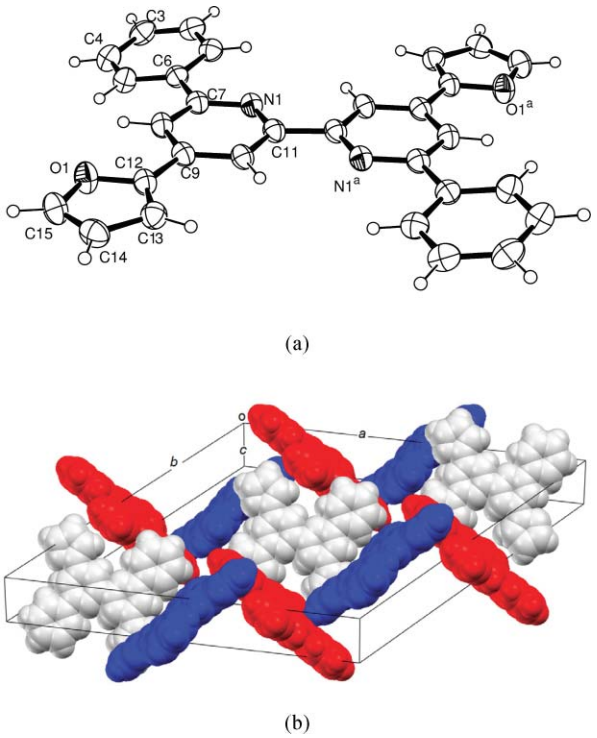

Fig. 4 (a) Molecular structure of **5**, with ellipsoids plotted at the 40% level. Selected bond parameters (Å and °): C11–C11^{a} 1.486(4), C6–C7 1.490(3), C9–C12 1.461(3), O1–C12 1.375(2), O1–C15 1.370(3), C12–C13 1.353(3), C13–C14 1.431(3), C14–C15 1.340(4); C12–O1–C15 106.9(2) (symmetry code a = 1 − *x*, 1 − *y*, 1 − *z*). (b) Packing of molecules of **5** in the unit cell.

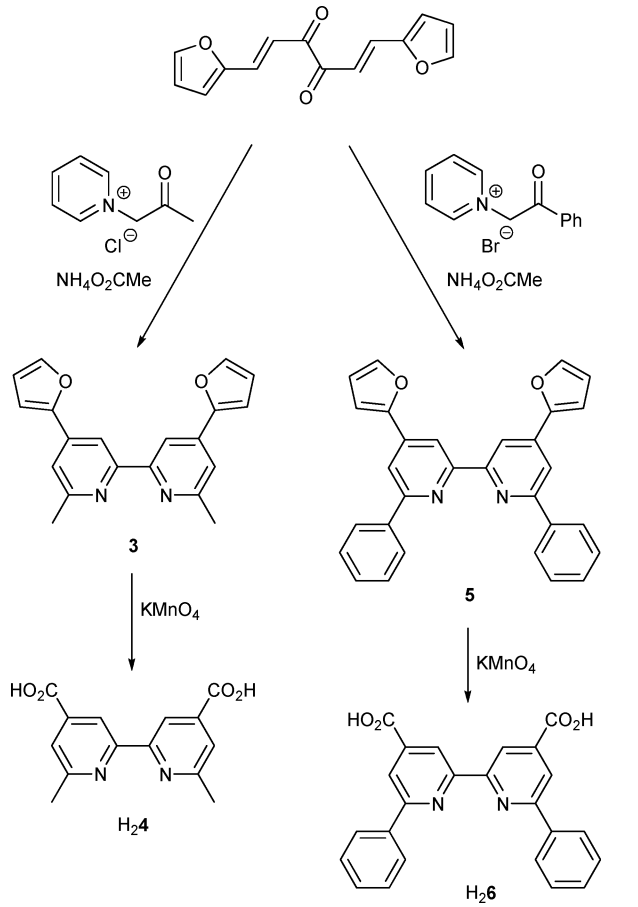

Scheme 2 Synthetic strategy for the formation of ligands H_2**4** and H_2**6**.

furan rings is 10.3(1)°, while in **5** it is 1.0(1)°. In **5**, the phenyl ring is twisted 10.7(1)° out of the plane of the pyridine ring to which it is bonded. Compounds **3** and **5** crystallise in orthorhombic (*Pcab*) and trigonal ($R\bar{3}$) space groups, respectively. In **3**, the principal packing forces are π-stacking interactions between bpy units. Pairs of pyridine rings in adjacent molecules are aligned so as to generate an offset stack (Fig. 3(b)), the distance between rings containing atoms N1 and N1^{i} being 3.39 Å, symmetry code i = 1 − *x*, −*y*, 1 − *z*). The dominant attractive forces between molecules of **5** involve weak edge-to-face π-interactions and $N_{pyridine}\cdots H\text{–}C_{furan}$ non-classical hydrogen bonds, and are in stark contrast to the π-stacking observed in **3**. The edge-to-face π-interactions feature both phenyl⋯phenyl and furan⋯furan contacts. The shortest phenyl⋯phenyl contact is C3⋯H51^{i}–C5^{i} (2.81 Å, symmetry code i = $\frac{2}{3}$ + *x* + *y*, $\frac{1}{3}$ + *x*, 1$\frac{1}{3}$ − *z*); the distance from the ring centroid to H51^{i} is 3.19 Å. Although not directly aligned, each C13–H131 bond points towards the C14–C15 π-bond of an adjacent furan ring (C13–H131⋯C15^{ii} = 3.02, C13–H131⋯C14^{ii} = 3.46 Å, symmetry code ii = $\frac{1}{3}$ − *x* + *y*, $\frac{2}{3}$ − *x*, −$\frac{1}{3}$ + *z*), and these weak interactions complement the edge-to-face aromatic interactions. The relative orientations of planar molecules of **5** that follow from the plethora of edge-to-face interactions place each nitrogen atom within close proximity of a furan hydrogen atom (N1⋯H151^{iii}C15^{iii} = 2.68 Å, N1⋯C15^{iii} = 3.605(4) Å, N1⋯H151^{iii}–C15^{iii} = 170°; symmetry code iii = $\frac{2}{3}$ + *x* + *y*, $\frac{1}{3}$ + *x*, $\frac{1}{3}$ − *z*). The high symmetry that crystallisation in the $R\bar{3}$ space group imparts on packing of molecules of **5** and the dominance of edge-to-face interactions are illustrated in Fig. 4(b).

Compounds **3** and **5** were oxidised to dicarboxylic acids H_2**4**[11] and H_2**6** (Scheme 2) using $KMnO_4$. The highest mass peak in the ESI mass spectrum of H_2**6** appeared at *m*/*z* 397.2 and was assigned to $[M + H]^+$. The NMR spectra of H_2**6** were recorded in CF_3CO_2D because the compound is not soluble in common organic solvents. Although it is difficult to compare the ^{1}H NMR spectra of **5** in $CDCl_3$ and H_2**6** in CF_3CO_2D (which may be protonated, see below), the significant changes in chemical shift for protons H^{A3} (δ 8.82 to 9.22 ppm) and H^{A5} (δ 8.07 to 9.00 ppm), and the disappearance of signals for the furan ring, confirm the replacement of the substituent in the 4- and 4′-positions of the bpy unit. In the ^{13}C NMR spectrum, a signal at δ 169.2 ppm was assigned to the carboxylic acid carbon atom. Single crystals of H_2**4** suitable for a X-ray diffraction study were grown from a methanol solution of the compound, and the centrosymmetric structure is shown in Fig. 5. The *trans*-configuration is as expected, and the molecule is planar (maximum deviation of a framework atom from the least squares plane through the molecule is 0.07 Å for C3). The difference in C5–O1 and C5–O2 bond distances (see figure caption) is consistent with carboxylic acid (rather than carboxylate) functionalities. The *trans*-arrangement of the two CO_2H groups is ideal for the formation of hydrogen-bonded polymeric chains (O1H1⋯O2^{i} = 1.78, O1⋯O2^{i} = 2.645(2) Å, O1–H1⋯O2^{i} = 177°, symmetry code i = 1 − *x*, 1 − *y*, 1 − *z*), and Fig. 6(a) illustrates that these all run in the same direction through the lattice. Adjacent chains assemble into sheets (Fig. 6(b)) by virtue of C=O⋯H_{methyl} attractive contacts

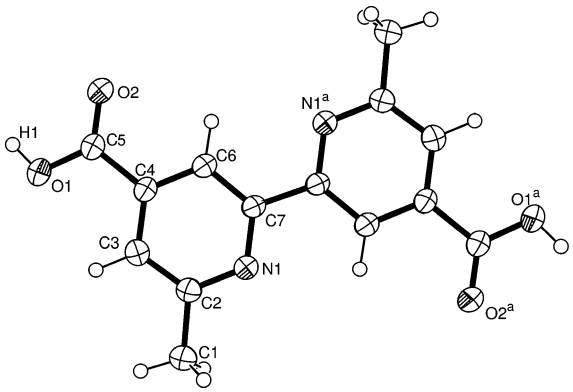

Fig. 5 Molecular structure of H_2**4**, with ellipsoids plotted at the 50% level. Selected bond parameters (Å and °): C4–C5 1.489(3), O2–C5 1.234(3), O1–C5 1.306(3), C7–C7^a 1.482(4), C1–C2 1.496(3); C4–C5–O1 115.8(2), C4–C5–O2 121.2(2), O1–C5–O2 122.9(2) (symmetry code a = $-x, -y, -z$).

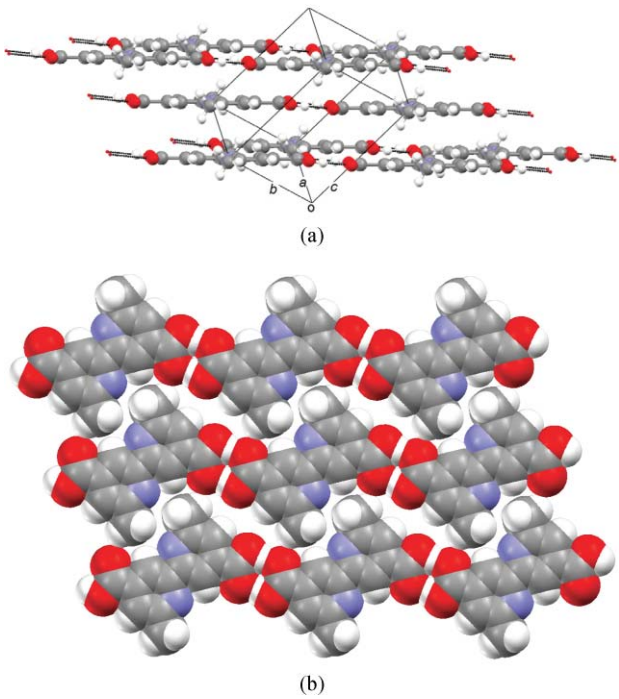

Fig. 6 (a) Hydrogen-bonded polymeric chains of H_2**4** molecules. (b) Adjacent chains assemble into 2D sheets.

(O2···H13^{ii}C1^{ii} = 2.60 Å, O2···C1^{ii} = 3.428(3) Å, O2···H13^{ii}–C1^{ii} = 143°, symmetry code ii = $-1 + x, 1 + y, z$). A methyl group from an adjacent molecule nestles into the cavity defined in Fig. 5 by atoms O2, C6–H61 and N1^a.

Crystals of [H_3**6**][CF_3CO_2]·2CF_3CO_2H were grown over a period of two days by dissolving the ligand in CF_3CO_2H and placing the vial containing the solution into a sample bottle containing a small amount of water. Fig. 7 shows the structure of the [H_3**6**]$^+$ cation. The bpy unit adopts a *cis*-conformation, consistent with protonation at one of the nitrogen atoms and the formation of an N–H···N hydrogen bond (the H atom being located in the difference map). The angle between the least squares planes of the two pyridine rings is 1.7(1)°. The difference between the two

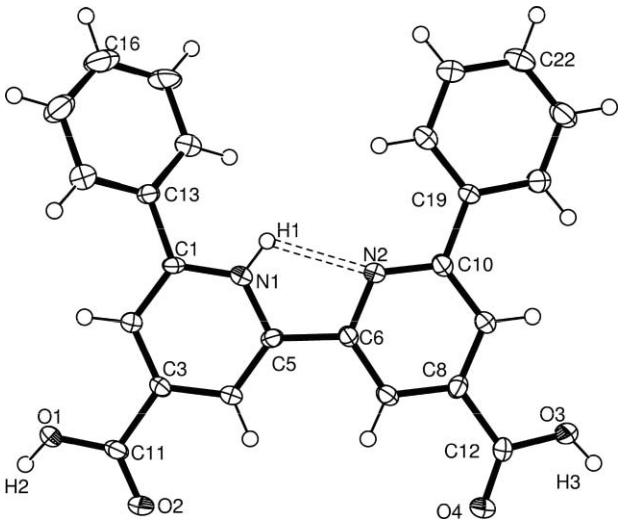

Fig. 7 Molecular structure of the [H_3**6**]$^+$ cation in [H_3**6**][CF_3CO_2]·2CF_3CO_2H; ellipsoids are plotted at the 50% level. Selected bond parameters (Å and °): O1–C11 1.304(3), O2–C11 1.203(3), O3–C12 1.307(3), O4–C12 1.204(3), N1···N2 2.599(3); O1–C11–O2 125.5(2), O3–C12–O4 123.7(2).

C–O bond distances in each carboxylic acid group (see caption to Fig. 7) confirms the protonation state. One phenyl substituent is twisted out of the plane of the bpy unit more than the other (angles between the least squares planes of rings containing atoms N1 and C13, and N2 and C19 are 31.3(1) and 7.2(1)°, respectively). Although the distance between the least squares planes through the bpy units of symmetry-related molecules in the triclinic unit cell is only 3.39 Å, there is little overlap of the rings and π-stacking interactions are therefore negligible. Packing within the lattice is controlled primarily by hydrogen bonding as illustrated in Fig. 8. The [CF_3CO_2]$^-$ ion and CF_3CO_2H solvate molecules are distinguished by a comparison of the C–O bond distances: C29–O9 and C29–O10 =1.221(3) and 1.249(3) Å, respectively, C25–O5 and C25–O6 = 1.195(4) and 1.287(4) Å, respectively, and C27–O7 and C27–O8 = 1.189(4) and 1.294(4) Å, respectively. The [CF_3CO_2]$^-$ ion and one of the CF_3CO_2H molecules are disordered. In the anion, each F atom position has been modelled over two sites with 65 and 35% occupancies. In the CF_3CO_2H molecule, two of the F atoms are disordered, and each position has been modelled over two sites with 70 and 30% occupancies.

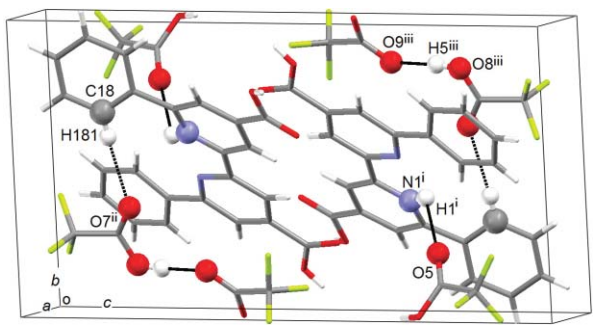

Fig. 8 Hydrogen bonding between cations, anions and solvate molecules in [H_3**6**][CF_3CO_2]·2CF_3CO_2H. Symmetry codes: i = $1 - x, 1 - y, 1 - z$; ii = $1 - x, -y, 1 - z$; iii = $x, 1 + y, z$.

Copper(I) complexes

Copper(I) complexes of ligands **3** and **5** were prepared by treating $[Cu(CH_3CN)_4][PF_6]$ with each ligand, and the hexafluoridophosphate salts of $[Cu(\mathbf{3})_2]^+$ and $[Cu(\mathbf{5})_2]^+$ were isolated as red and green solids, respectively, in moderate to good yields. The electronic absorption spectra of acetonitrile solutions of $[Cu(\mathbf{3})_2][PF_6]$ and $[Cu(\mathbf{5})_2][PF_6]$ exhibited MLCT bands at 493 and 587 nm, respectively, consistent with the observed colours. The spectra also showed intense, higher energy absorptions assigned to ligand centred $\pi^* \leftarrow \pi$ transitions. Each complex is redox active, and undergoes a reversible Cu^+/Cu^{2+} process at +0.29 V for $[Cu(\mathbf{3})_2][PF_6]$, and +0.27 V for $[Cu(\mathbf{5})_2][PF_6]$. The highest mass peaks in the ESI mass spectra of $[Cu(\mathbf{3})_2][PF_6]$ and $[Cu(\mathbf{5})_2][PF_6]$ corresponded to $[M - PF_6]^+$ (*m*/*z* 695.8 for $[Cu(\mathbf{3})_2]^+$ and 943.0 for $[Cu(\mathbf{5})_2]^+$). Coordination of ligand **3** to copper(I) results in only small changes to the ^{1}H NMR spectrum (both in $CDCl_3$). Similarly, on going from **5** (in $CDCl_3$) to $[Cu(\mathbf{5})_2]^+$ (in CD_2Cl_2), the chemical shifts of the signals assigned to the bpy and furan protons undergo small perturbations. However, the signals for the phenyl protons are significantly shifted to lower frequency (H^{C2} from δ 8.23 to 7.58 ppm, H^{C3} from δ 7.57 to 6.91 ppm, and H^{C4} from 7.49 to 7.06 ppm). This is a consequence of the shielding resulting from each phenyl substituent lying over the π-cloud of a bpy domain of the second ligand, enforced by the near tetrahedral copper(I) coordination sphere (see structural discussion below).

The electronic spectra of $[Cu(\mathbf{3})_2][PF_6]$ and $[Cu(\mathbf{5})_2][PF_6]$ exhibit intense absorptions in the UV region assigned to ligand-based $\pi^* \leftarrow \pi$ transitions, in addition to absorptions arising from MLCT transitions (493 nm for $[Cu(\mathbf{3})_2]^+$ and 432 and 587 nm for $[Cu(\mathbf{5})_2]^+$). The introduction of phenyl substituents in the 6- and 6′-positions results in the observation of a second MLCT band, extends the range of the absorption spectrum into the red.[27]

Crystals of $[Cu(\mathbf{3})_2][PF_6]$ suitable for X-ray analysis were grown by slow diffusion of Et_2O into a $CHCl_3$ solution of the complex. The structure of the $[Cu(\mathbf{3})_2]^+$ cation is shown in Fig. 9 and confirms that the two ligands are close to being orthogonal (angle between the least squares planes through the two bpy units = 81.11(5)°); the bite angle of each bpy ligand is ≈81°. Two of the furan rings are disordered and have been modelled with O/C mixed occupancy sites (O3 and C54 75% occupancy, and C134 and O30 25%; O4 and C58 70% occupancy, and C138 and O40 30%). Each ligand is close to being planar, with the maximum deviation being for the furan ring containing atom O2 (angle between the least squares planes of rings with O2 and N2 = 14.1(1)°). The packing of the cations is noteworthy. One near-planar ligand stacks over a ligand of an adjacent cation. The interplane distances are appropriate for π-stacking (distances between planes containing N1/N2 and $N1^i/N2^i$ = 3.43 Å, N3/N4 and $N3^{ii}/N4^{ii}$ = 3.37 Å, symmetry codes: i = 1 − *x*, 1 − *y*, 1 − *z*; ii = 2 − *x*, −*y*, −*z*). However, the two ligands of each complex interact with their neighbours in different ways. Stacking between ligands containing N1/N2 and $N1^i/N2^i$ involves the whole face of each ligand. In contrast, half of each N3/N4 ligand stacks with half of a symmetry-related ligand in an adjacent molecule; Fig. 10(a) shows the stacking involving pyridine rings N3 ··· $N3^{ii}$ and illustrates that face-to-face pyridine ··· furan stacking occurs. The remaining half of the ligand stacks with another cation (represented as N4 ··· $N4^{iii}$, symmetry code iii = 1 − *x*, 1 − *y*, −*z*) leading to the overall evolution of stacked chains of cations running in parallel directions through the lattice (Fig. 10(b)). The $[PF_6]^-$ ions reside in the cavities between the cations, and there are extensive C–H ··· F–P weak interactions.

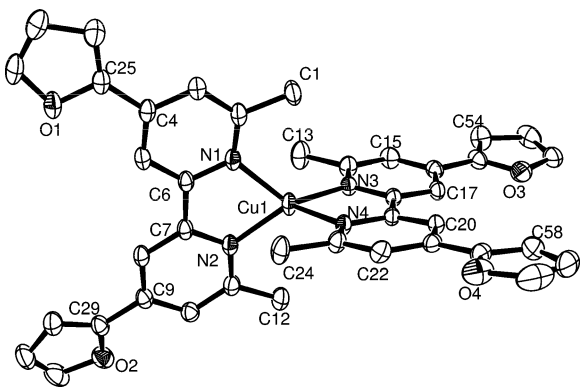

Fig. 9 Molecular structure of the $[Cu(\mathbf{3})_2]^+$ cation in $[Cu(\mathbf{3})_2][PF_6]$; ellipsoids are plotted at the 40% level and H atoms are omitted. The furan rings containing O3 and O4 are disordered and only the major occupancy atoms are shown (see text). Selected bond parameters (Å and °): Cu1–N1 2.024(2), Cu1–N2 2.011(2), Cu1–N3 2.000(2), Cu1–N4 2.026(2); N1–Cu1–N2 81.27(7), N1–Cu1–N3 130.31(7), N2–Cu1–N3 128.77(7), N1–Cu1–N4 113.72(6), N2–Cu1–N4 126.03(6), N3–Cu1–N4 81.94(6).

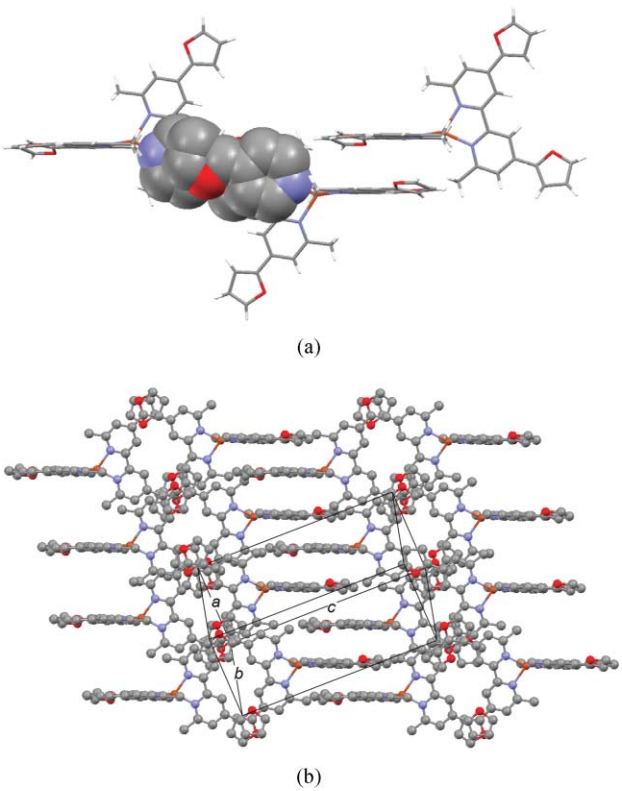

Fig. 10 Packing of cations in $[Cu(\mathbf{3})_2][PF_6]$.

The copper(I) complexes of $H_2\mathbf{2}$, $H_2\mathbf{4}$ and $H_2\mathbf{6}$ were prepared by the addition of copper(II) sulfate to aqueous solutions of the sodium salts of the acids, followed by reduction with ascorbic acid.[8] After work-up in aqueous HCl, $[Cu(H_2\mathbf{2})_2]Cl$ and $[Cu(H_2\mathbf{4})_2]Cl$ were isolated as red solids, and $[Cu(H_2\mathbf{6})_2]Cl$ as a

green solid. The cations in $[Cu(H_2\mathbf{2})_2]Cl$ and $[Cu(H_2\mathbf{4})_2]Cl$ are isomers, and ESI mass spectra showed ions corresponding to $[CuL_2]^+$ at m/z 607. The electronic spectra of methanol solutions of $[Cu(H_2\mathbf{2})_2]Cl$ and $[Cu(H_2\mathbf{4})_2]Cl$ exhibit MLCT bands at 482 and 483 nm, respectively, in addition to more intense, higher energy ligand-based absorptions arising from $\pi^* \leftarrow \pi$ transitions (Fig. 11). Upon formation of the complexes, signals in the ^1H NMR spectra undergo minor perturbations, although the change in solvent from DMSO-d_6 to CD_3OD makes detailed comparisons difficult. The elemental analysis of the bulk sample of $[Cu(H_2\mathbf{6})_2]Cl$ confirmed the formulation, but mass spectrometric and solution spectroscopic characterisation of $[Cu(H_2\mathbf{6})_2]Cl$ proved to be difficult. Attempts to obtain an ESI mass spectrum of the complex led only to the observation of a peak envelope at m/z 396 assigned to the free ligand. Unlike $[Cu(H_2\mathbf{2})_2]Cl$ and $[Cu(H_2\mathbf{4})_2]Cl$ which are slightly soluble in MeOH, $[Cu(H_2\mathbf{6})_2]Cl$ is insoluble in water and common organic solvents with the exception of DMSO. The ^1H NMR spectrum of a DMSO-d_6 solution of $[Cu(H_2\mathbf{6})_2]Cl$ showed only broad peaks at room temperature. Initially we wondered if this were due to restricted bond rotation around the C_{py}–C_{phenyl} bond but the signals did not sharpen upon increasing the temperature of the solution. Since DMSO is not ideal for crystal growth at room temperature, we attempted to grow crystals of $[Cu(H_2\mathbf{6})_2]Cl$ by leaving the crude reaction mixture (still containing an excess of NaOH) to stand for several days. Single crystals of $Na_3[Cu(\mathbf{6})_2]$ (see below) were isolated. The sodium salt was water-soluble, and the ^1H NMR spectrum of a D_2O solution of the complex was well-resolved. We noted earlier that on going from **5** to $[Cu(\mathbf{5})_2]^+$, signals for the phenyl protons shift to lower frequency, and the same phenomenon is observed on going from $H_2\mathbf{6}$ (in CF_3CO_2D) to $[Cu(\mathbf{6})_2]^{3-}$ (in D_2O) (H^{C2} from δ 8.19 to 6.99 ppm, H^{C3} from δ 7.77 to 6.40 ppm, and H^{C4} from δ 7.82 to 6.49 ppm). Preliminary structural data for $Na_3[Cu(\mathbf{6})_2].nH_2O$ confirm that the coordination geometry of the copper(I) centre is distorted tetrahedral and that each phenyl substituent lies over the bpy unit of the second ligand, consistent with the shielding effects noted in the ^1H NMR spectrum. Unfortunately, the structure was severely disordered with respect to the positions of the Na^+ ions and solvate molecules, and attempts to grow better quality crystals were unsuccessful.

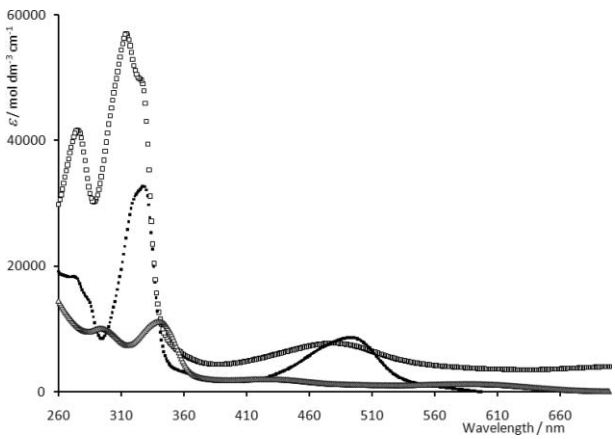

Fig. 11 Comparison of part of the electronic spectra of $[Cu(H_2\mathbf{2})_2]Cl$ (□, MeOH), $[Cu(H_2\mathbf{4})_2]Cl$ (■, MeOH) and $Na_3[Cu(\mathbf{6})_2]$ (△, H_2O, lowest extinction coefficients).

Attempts to obtain the electronic spectrum of a DMSO solution of $[Cu(H_2\mathbf{6})_2]Cl$ were hampered by the fact that the complex is not stable in this solvent. Therefore, the spectrum of an aqueous solution of $Na_3[Cu(\mathbf{6})_2]$ was recorded. In addition to high energy absorptions assigned to ligands-centred $\pi^* \leftarrow \pi$ transitions, the spectrum exhibited two MLCT bands at 437 and 608 nm. The spectrum is compared with those of $[Cu(H_2\mathbf{2})_2]Cl$ and $[Cu(H_2\mathbf{4})_2]Cl$ in Fig. 11, and illustrates the decrease in intensity of the MLCT bands on going from the complexes with ligands $H_2\mathbf{2}$ or $H_2\mathbf{4}$ to $[\mathbf{6}]^-$, and, by inference, $H_2\mathbf{6}$.

Crystals of $4[Cu(H_2\mathbf{2})(H\mathbf{2})]\cdot 3H_2O$ grew after a methanol solution of $[Cu(H_2\mathbf{2})_2]Cl$ had been standing at room temperature for several weeks. The molecular structure is shown in Fig. 12 and selected bond parameters are given in the caption. The disordering leads to large estimated standard deviations, but the bond distances are consistent with the protonation states shown in the figure. The fully protonated ligand is ordered, while the CO_2H and CO_2 units of the second ligand are disordered and have been modelled (each with the CO_2 units constrained to being planar) over two sites, each with equal occupancy. One methyl group is also disordered (C28 in Fig. 12) and has been modelled over two sites of fractional occupancies of 75% and 25%. The compound crystallises as a hydrate, and one water molecule resides on a two-fold axis. The copper(I) centre is in the expected pseudo-tetrahedral environment, the angle between the least squares planes of the two bpy units being 84.49(7)°. The packing of $[Cu(H_2\mathbf{2})(H\mathbf{2})]$ molecules is worthy of note and involves both π-stacking between bpy domains and extensive hydrogen bonding between carboxylate and carboxylic acid groups. The bpy unit containing N1 and N2 stacks over that containing $N3^i$ and $N4^i$ (symmetry code i = x, $1-y$, $\frac{1}{2}+z$) of an adjacent molecule. The stacking is not ideal, and while the bpy units overlap effectively, their planes are not parallel. The distance from the centroids of the rings containing N1 and N2 to the least squares plane through the bpy unit with

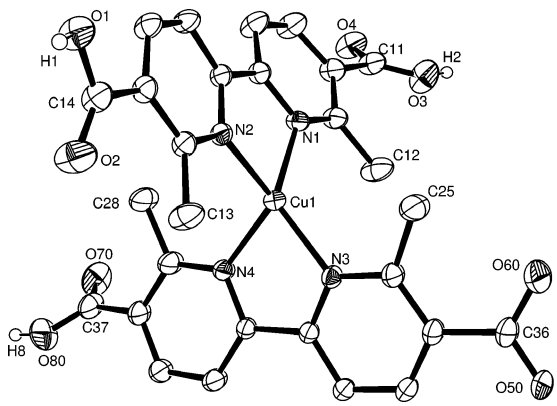

Fig. 12 Structure of the $[Cu(H_2\mathbf{2})(H\mathbf{2})]$ molecule in $4[Cu(H_2\mathbf{2})(H\mathbf{2})]\cdot 3H_2O$; H atoms except those in the CO_2H groups are omitted, and ellipsoids are plotted at the 30% level. For disordered atoms, one (if 50 : 50) or major occupancy (for C28) sites only are shown. Selected bond parameters (Å and °): Cu1–N1 2.057(1), Cu1–N2 2.045(1), Cu1–N3 2.036(1), Cu1–N4 2.052(2), C11–O3 1.272(3), C11–O4 1.228(3), C14–O1 1.311(3), C14–O2 1.211(3), C36–O50 1.25(3), C36–O60 1.29(2), C37–O70 1.208(8), C37–O80 1.283(8); N1–Cu1–N2 81.30(6), N1–Cu1–N3 128.59(6), N2–Cu1–N3 133.40(6), N1–Cu1–N4 121.97(6), N2–Cu1–N4 115.34(6), N3–Cu1–N4 81.12(6), O3–C11–O4 127.3(2), O1–C14–O2 124.1(2), O50–C36–O60 118(2), O70–C37–O80 125.7(6).

N3^{i} and N4^{i} are 3.24 and 3.47 Å, respectively. In contrast, for the N3/N4 bpy unit, only the ring containing N3 is involved in significant π-stacking. The interaction occurs with the N3^{ii} ring across an inversion centre with the distance between least squares planes through the pyridine rings being 3.46 Å. The π-stacked interactions therefore operate in orthogonal directions to produce a network that is reinforced by hydrogen bonding between carboxylates and carboxylic acids. Every CO_2^- or CO_2H group is involved, as well as the water molecules, resulting in a rigid network (Fig. 13).

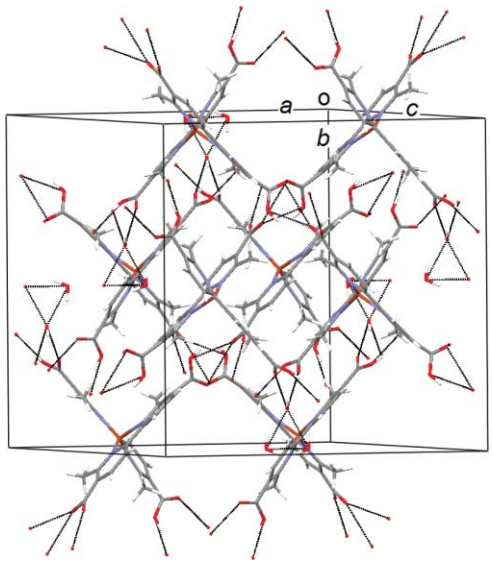

Fig. 13 Crystal packing in 4[Cu(H$_2$**2**)(H**2**)]·3H$_2$O involves extensive π-stacking and hydrogen bonding in orthogonal directions.

Performance of DSCs

Prior to our recent communication concerning the efficient performances of DSCs with carboxylate-derivatized $[CuL_2]^+$ complexes in which L = H$_2$**4**, **7**, H$_2$**8** and **9** (Scheme 3),[5] reports of photosensitization by copper(I) dyes were surprisingly few.[28–30] Here, we describe a comparison of the performances of DSCs using the copper(I) dyes H$_2$**2**, H$_2$**4** and H$_2$**6**. Each is functionalized with carboxylic acids, and is therefore expected to bind to TiO_2. We have also constructed DSCs using **3** as the dye in order to assess the binding capabilities of the furan functionality.

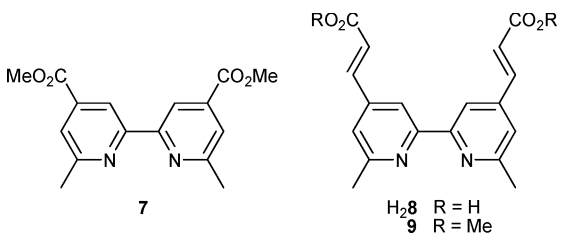

Scheme 3 Ligands previously incorporated into copper(I)-based solar cells in addition to H$_2$**4**.[5]

The characteristics of these DSCs and of the standard dye N719 were measured using our modified scanning electrochemical microscope system and are given in Table 1.

Like $[Cu(H_2\mathbf{4})_2]^+$,[5] complexes $[Cu(H_2\mathbf{2})_2]^+$ and $[Cu(H_2\mathbf{6})_2]^+$ bind strongly to TiO_2 nanoparticles, giving good dye-modified surfaces. To the best of our knowledge, no dyes bearing furan functionalities as the anchoring group have previously been reported. After being immersed in a $CHCl_3$ solution of $[Cu(\mathbf{3})_2][PF_6]$ for several hours, the TiO_2 nanoparticles on the conducting glass slides were coloured indicating chemisorption of the dye. The UV-VIS spectrum exhibited an MLCT band at 494 nm consistent with the solution spectrum of the complex (Table 1). Although this is consistent with $[Cu(\mathbf{3})_2]^+$ binding to TiO_2 nanoparticles through the furan *O*-donors, we cannot rule out the possibility of oxidation of the furan functionalities to carboxylic acids.

The lower performance of the DSCs constructed with H$_2$**6** compared with H$_2$**4** is a combination of the lower absorptivity of the complex and lower adsorption on the oxide surface.

Conclusions

In this paper, we have described systematic approaches to 6,6′-disubstituted-2,2′-bipyridine ligands bearing carboxylic acid substituents at the 4,4′- or 5,5′-positions. Copper(I) complexes with these ligands have been prepared and a preliminary assessment of their utilisation as dye-sensitizers in copper-based DSCs has been made.

Acknowledgements

We thank the University of Basel, the Swiss National Science Foundation, the Swiss Nanoscience Institute and the EU (HETEROMOLMAT) for financial support. Dr Daniel Häussinger is thanked for recording the 600 MHz NMR spectra, and we acknowledge the assistance of Dr Biljana Bozic-Weber in recording UV-VIS spectroscopic and electrochemical data.

References

1 M. K. Nazeeruddin and M. Grätzel, *Struct. Bonding*, 2007, **123**, 113.
2 M. Grätzel, *Inorg. Chem.*, 2005, **44**, 6841.
3 A. S. Polo, M. K. Itokazu and N. Y. M. Iha, *Coord. Chem. Rev.*, 2004, **248**, 1343.
4 S. Ardo and G. J. Meyer, *Chem. Soc. Rev.*, 2009, **38**, 115.
5 T. Bessho, E. C. Constable, M. Grätzel, A. Hernandez Redondo, C. E. Housecroft, W. Kylberg, Md. K. Nazeeruddin, M. Neuburger and S. Schaffner, *Chem. Commun.*, 2008, 3717.
6 W. W. Brandt, F. P. Dwyer and E. D. Gyarfa, *Chem. Rev.*, 1954, **545**, 959.
7 See for exampleN. Shan, A. D. Bond and W. Jones, *Cryst. Eng.*, 2002, **5**, 9; C. B. Aakeröy, J. Desper and J. F. Urbina, *CrystEngComm*, 2005, **7**, 193; B. R. Bhogala, S. Basavoju and A. Nangia, *Cryst. Growth Des.*, 2005, **5**, 1683; W.-H. Wang, P.-H. Xi, X.-Y. Su, J.-B. Lan, Z.-H. Mao, J.-S. You and R.-G. Xie, *Cryst. Growth Des.*, 2007, **7**, 741; C. B. Aakeröy, M. E. Fasulo and J. Desper, *Mol. Pharm.*, 2007, **4**, 317; B. R. Bhogala and A. Nangia, *New J. Chem.*, 2008, **32**, 800; T. R. Shattock, K. K. Arora, P. Vishweshwar and M. J. Zaworotko, *Cryst. Growth Des.*, 2008, **8**, 4533; M. Byres, P. J. Cox, G. Kay and E. Nixon, *CrystEngComm*, 2009, **11**, 135and references therein.
8 S. Sakaki, H. Ishikura, K-i. Kuraki, K-j. Tanaka, T. Satoh, T. Arai and T. Hamada, *J. Chem. Soc., Dalton Trans.*, 1997, 1815.
9 P. Karrer, Ch. Cochand and N. Neuss, *Helv. Chim. Acta*, 1946, **29**, 1836.
10 F. Kröhnke, *Synthesis*, 1976, 1.
11 V. M. Mukkala and J. J. Kankare, *Helv. Chim. Acta*, 1992, **75**, 1578.
12 COLLECT Software, Nonius BV 1997–2001.
13 Z. Otwinowski and W. Minor, *Methods Enzymol.*, 1997, **276**, 307.

14 A. Altomare, G. Cascarano, G. Giacovazzo, A. Guagliardi, M. C. Burla, G. Polidori and M. Camalli, *J. Appl. Crystallogr.*, 1994, **27**, 435.
15 P. W. Betteridge, J. R. Carruthers, R. I. Cooper, K. Prout and D. J. Watkin, *J. Appl. Crystallogr.*, 2003, **36**, 1487.
16 I. J. Bruno, J. C. Cole, P. R. Edgington, M. K. Kessler, C. F. Macrae, P. McCabe, J. Pearson and R. Taylor, *Acta Crystallogr., Sect. B*, 2002, **58**, 389.
17 L. J. Farrugia, *J. Appl. Crystallogr.*, 1997, **30**, 565.
18 G. M. Badger and W. H. F. Sasse, *Adv. Heterocycl. Chem.*, 1963, **2**, 179.
19 G. M. Badger and W. H. F. Sasse, *J. Chem. Soc.*, 1956, 616.
20 G. R. Desiraju and T. Steiner, *The Weak Hydrogen Bond*, Oxford University Press, Oxford, 1999.
21 T. Steiner, *Angew. Chem., Int. Ed.*, 2002, **41**, 48.
22 G. R. Desiraju, *Chem. Commun.*, 2005, 2995.
23 G. R. Desiraju, *Acc. Chem. Res*, 2002, **35**, 565.
24 M. Nishio, M. Hirota and Y. Umezawa, *The CH/π Interaction: Evidence, Nature, and Consequences*, Wiley, Weinheim, 1998.
25 M. Nishio, *CrystEngComm*, 2004, **6**, 130.
26 J. Husson, M. Beley and G. Kirsch, *Tetrahedron Lett.*, 2003, **44**, 1767.
27 C. O. Dietrich-Buchecker, P. A. Marnot, J.-P. Sauvage, J. R. Kirchhoff and D. R. McMillin, *J. Chem. Soc., Chem. Commun.*, 1983, 513.
28 N. Alonso-Vante, V. Ern, P. Chartier, C. O. Dietrich-Buchecker, D. R. McMillin, P. A. Marnot and J.-P. Sauvage, *New J. Chem.*, 1983, **7**, 3.
29 N. Alonso-Vante, J.-F. Nierengarten and J.-P. Sauvage, *J. Chem. Soc., Dalton Trans.*, 1994, 1649.
30 S. Sakati, T. Kuroki and T. Hamada, *J. Chem. Soc., Dalton Trans.*, 2002, 840.

